TECHNICAL RESEARCH REPORT

Ripple Analysis in Ferret Primary Auditory Cortex. II. Topographic and Columnar Distribution of Ripple Response Parameters

by H. Versnel, N. Kowalski and S.A. Shamma

T.R. 94-21

Sponsored by
the National Science Foundation
Engineering Research Center Program,
the University of Maryland,
Harvard University,
and Industry

Report Documentation Page

Form Approved
OMB No. 0704-0188

1. REPORT DATE	2. REPORT TYPE	3. DATES COVERED
1994		**00-00-1994 to 00-00-1994**

4. TITLE AND SUBTITLE	5a. CONTRACT NUMBER
Ripple Analysis in Ferret Primary Auditory Cortex. II. Topographic and Columnar Distribution of Ripple Response Parameters.	5b. GRANT NUMBER
	5c. PROGRAM ELEMENT NUMBER
6. AUTHOR(S)	5d. PROJECT NUMBER
	5e. TASK NUMBER
	5f. WORK UNIT NUMBER
7. PERFORMING ORGANIZATION NAME(S) AND ADDRESS(ES) **Department of Electrical Engineering,Institute for Systems Research,University of Maryland,College Park,MD,20742**	8. PERFORMING ORGANIZATION REPORT NUMBER
9. SPONSORING/MONITORING AGENCY NAME(S) AND ADDRESS(ES)	10. SPONSOR/MONITOR'S ACRONYM(S)
	11. SPONSOR/MONITOR'S REPORT NUMBER(S)

12. DISTRIBUTION/AVAILABILITY STATEMENT
Approved for public release; distribution unlimited

13. SUPPLEMENTARY NOTES

14. ABSTRACT
see report

15. SUBJECT TERMS

16. SECURITY CLASSIFICATION OF:			17. LIMITATION OF ABSTRACT	18. NUMBER OF PAGES	19a. NAME OF RESPONSIBLE PERSON
a. REPORT **unclassified**	b. ABSTRACT **unclassified**	c. THIS PAGE **unclassified**		**27**	

Ripple Analysis in Ferret Primary Auditory Cortex. II. Topographic and Columnar Distribution of Ripple Response Parameters.

Huib Versnel[a], *Nina Kowalski*[b], *and Shihab A. Shamma*[c]

(a) Institute for Systems Research, University of Maryland, College Park, MD 20742.

(b) Electrical Engineering Department and Institute for Systems Research, University of Maryland, College Park, MD 20742.

(c) Electrical Engineering Department, University of Maryland Institute for Advanced Computer Studies, and Institute for Systems Research. University of Maryland, College Park, MD 20742.

ABSTRACT

We examined the columnar and topographic distribution of response parameters using spectral ripples and tonal stimuli in the primary auditory cortex (AI) of the barbiturate-anesthetized ferret. The ripple stimuli consisted of broadband stimuli (1-20 kHz) with sinusoidally modulated spectral envelopes. Responses to ripples were parametrized in terms of characteristic ripple Ω_o (ripple frequency where the magnitude of the ripple transfer function is maximal, i.e., where the cell responds best) and characteristic phase Φ_o (intercept of the phase of the ripple transfer function, i.e., phase where the cell responds best). The response area (measured with tones) was parametrized in terms of its excitatory bandwidth at 20 dB above threshold (BW20), and its asymmetry as reflected by the directional sensitivity index (C) to frequency-modulated (FM) tones. Columnar organization for the above four parameters was investigated in 66 single units from 23 penetrations. It was confirmed for Ω_o, Φ_o, and the C index, but it appeared to be ambiguous for BW20. The response parameters measured from multiunit recordings corresponded closely to those obtained from single units in the same cluster. In a local region, most cells exhibited closely matched response fields (RFs, inverse Fourier transformed ripple transfer function) and response areas (measured with two-tone stimuli), and had correspondingly similar response parameters to ripples and tones. The topographic distribution of the response parameters across the surface of AI was studied with multiunit recordings in four animals. In all maps, systematic patterns or clustering of response parameters could be discerned along the isofrequency planes. The distribution of the characteristic ripple Ω_o exhibited two trends. First, along the isofrequency planes, it was largest near the center of AI, gradually decreasing towards the edges of the field where often a secondary maximum was found. The second trend occured along the tonotopic axis where the maximum Ω_o found in an isofrequency range increases with increasing BF. The tonal bandwidth BW20, which was inversely correlated with Ω_o, exhibited a similar topographic distribution along the tonotopic axis and the isofrequency planes. The distribution of the characteristic ripple phase, Φ_o, which reflects the asymmetry in the response field, showed a systematic order along the isofrequency axis. At the center of AI symmetric responses ($\Phi_o \approx 0$) predominated. Towards the edges, the RFs became more asymmetric with $\Phi_o < 0$ caudally, and $\Phi_o > 0$ rostrally. The asymmetric response types tended to cluster along repeated bands that paralleled the tonotopic axis. The FM directional sensitivity (C index, reflecting asymmetry of tonal response areas) tends to have similar trends along the isofrequency axis as Φ_o.

INTRODUCTION

Cells in the primary auditory cortex (AI) exhibit a rich variety of responses to complex stimuli. This has made it generally difficult to ascertain the functional relevance of any particular response property without additional supporting criteria. One such criterion is a specialized behavioral repertoire that can be directly related to the responses as in the echolocating bats (Suga 1984). Another useful criterion of functional relevance in less specialized mammals is the existence of an ordered spatial distribution of the responses, both columnar and across the surface of the cortex. This organizational principle has been the driving force behind most neurophysiological mappings of the auditory cortex, the visual cortex, and other sensory areas.

In AI, at least three different monaural response properties have been reported to be spatially and columnarly ordered. They are the tonotopic map (Merzenich et al. 1975), the broadening of the excitatory response bandwidth towards the edges of AI (Schreiner and Mendelson 1990; Heil et al. 1992a), and the ordered change in response area asymmetry along the isofrequency planes (Shamma et al. 1993). Other response properties which seem to be related to the latter two are spatially ordered as well, e.g., FM directional sensitivity (Heil et al. 1992b; Shamma et al. 1993; Mendelson et al. 1993) and intensity profiles (Phillips et al. 1985, 1993). An additional organization of binaural response properties has also been extensively studied (Middlebrooks et al. 1980).

These response parameters are usually measured using simple tonal stimuli. However, it is shown in the companion paper (Shamma et al. 1994) that they can also be predicted from responses to complex and broadband rippled spectra. Ripple responses appear to be correlated to tone responses. For instance, the response area bandwidth and asymmetry are correlated with the characteristic ripple (Ω_o) and phase (Φ_o) of its ripple transfer function. This correspondence suggests that ripple response features, as represented by Ω_o and Φ_o, might also be topographically ordered.

The aim of this paper is to establish whether spatially ordered maps of Ω_o, Φ_o, and other ripple response features exist in AI. In order to facilitate the recording of a large number of penetrations in each animal, all maps are constructed from multiunit recordings. This type of records is similar to single-unit records with respect to tone response features (Shamma et al. 1993), and here we compare the two types of records for ripple responses. Finally, the functional implications of such maps will be discussed, and their relationship to analogous organizational features in other sensory areas such as the visual cortex.

METHODS

Animal preparation

The ferrets were anesthetized with sodium pentobarbital (40 mg/kg). Anesthesia was maintained throughout the experiment by continuous intravenous infusion of pentobarbital. The ectosylvian gyrus, which includes the primary auditory cortex was exposed by craniotomy and the dura was reflected. The contralateral ear canal was exposed and partly resected, and subsequently a cone-shaped speculum containing a Sony MDR-E464 miniature speaker was sutured to the meatal stump. For details on the surgery see Shamma et al. (1993, 1994).

Acoustic stimuli

Acoustic stimuli consisted of pure tone stimuli (single and two-tone bursts, 200 ms duration, 10 ms rise- and fall-times, 50 ms intertone delay), FM sweeps (2 octaves around BF, at sweeping rates 50-250 octaves/s, two sweep directions) and broadband complex stimuli with rippled spectra. The latter consisted of 101 tones that were equally spaced along the logarithmic frequency axis and spanning 4.32 octaves such that the best frequency (BF) of the cell tested was covered (e.g., 1-20 kHz or 0.25-5 kHz). The envelope of the complex stimulus was modulated sinusoidally on logarithmic frequency and amplitude scales (for the mapping experiments the amplitude was typically 10 dB base-to-peak). For further details on the stimuli see Shamma et al. (1994).

Recordings

In 4 animals we performed mapping experiments, lasting up to 57 hours, in which recordings were made from multiunit clusters as described in Shamma et al. (1993). Briefly, in each animal, electrode penetrations were made orthogonal to the cortical surface. Our strategy was to maximize the number of such penetrations along the isofrequency planes. This necessarily limited the number of stimulus parameters tested in a given penetration. A mapping experiment typically consisted of 40–70 useful microelectrode penetrations spaced 100– 300 μm apart, and recordings were made at a depth of 350-600 μm. Excitatory onset responses to single tones at this depth are strongest. Previous histological examination of Nissl-stained sections showed that this depth corresponds to cortical layers III and IV in young adult ferrets (Shamma et al. 1993).

In 7 animals both multiunit and single-unit recordings were performed. In each animal about 10 penetrations were made, and in each penetration, up to 7 cells were studied. Recordings were made at various depths, ranging from 150 μm to 750 μm, in order to study columnar organization.

In multiunit recordings one cannot be certain that the number of events detected corresponds exactly to the number of spikes present. To avoid ambiguity, we shall strictly distinguish the single-unit and cluster records in our figures and discussion by using the term "response amplitude" to signify the number of events recorded in multiunit clusters. The term "spike count" will be reserved for single-unit records only.

Data analysis

The primary objective of the experiments reported here is to establish the topographic and columnar distribution of various response measures in AI. For all single-unit and cluster recordings, the response measures used are the same as those described in detail in the companion paper (Shamma et al. 1994). In this paper, we particularly discuss the following two parameters in respect to tonal stimuli: the excitatory bandwidth determined at 20 dB above BF threshold (BW20), and the directional sensitivity of frequency modulation (FM) sweeps. The measure of FM directional sensitivity (C index) is derived as follows:

$$C = \frac{R\downarrow - R\uparrow}{R\downarrow + R\uparrow} \tag{1}$$

where $R\uparrow$ and $R\downarrow$ are the spike counts or response amplitudes to the up and down sweeps, respectively.

The ripples are varied in phase (Φ) and ripple density or ripple frequency (Ω). Responses are measured with respect to their phase following (i.e., sinusoidal variation with Φ) and response curves consist of magnitude and Φ transfer functions. The response parameters derived from these transfer functions are the characteristic ripple (Ω_o) and the characteristic phase (Φ_o), respectively. The former parameter is the Ω at which the response is largest (i.e., the first harmonic of the AC component of the response), and the latter parameter is the constant phase shift in the phase function (which is in most instances linear, Shamma et al. 1994). Inverse Fourier transformation of the transfer functions yields a curve which resembles the response area as derived with tonal stimuli; this curve is defined the response field (RF).

Topographic representation of the data

In the ferret, AI is located on the ectosylvian gyrus. Its exact location, orientation, and particularly its width, varies from one animal to another.

In each mapping experiment, tonal and ripple response parameters were determined for numerous penetrations distributed across AI, and displayed using an arbitrary shading scheme, as indicated by the key next to each map. The resulting maps for each animal show the topographic distribution of the parameter values, along with a few isofrequency contours. Parameter values that were not measured at individual grid locations (separated by $\approx 50\mu$m) are determined by a weighted fill interpolation. Each grid location with a missing parameter value is assigned a Gaussian weighted average of the nearest experimentally determined values within five locations, while all experimentally determined values are preserved. The isofrequency contours were interpolated with a kernel smoothing algorithm, which does not preserve original values.

Estimate of columnar organization

In order to assess the extent of columnar organization with respect to response properties (as Ω_o and Φ_o), the scatter within columns is compared to the overall scatter. Theoretically, the total variance (square of standard deviation) is the sum of the variance within a column and the variance between columns (cf. Duda and Hart 1973).

$$Var_T = Var_W + Var_B \tag{2}$$

where Var_T is total variance, Var_W variance within, and Var_B variance between columns.

Generally, a significantly small ratio $\mathrm{Var}_W/\mathrm{Var}_T$ indicates a clustering per column. However, two sources of error affect this ratio. The first is measurement error that tends to increase Var_W and consequently the ratio $\mathrm{Var}_W/\mathrm{Var}_T$. The other source is sampling error that, like clustering, reduces this ratio. The sampling error is due to the small numbers of cells that could be tested in one column. The sampling error is estimated by performing tests with random entries instead of the measured ones.

RESULTS

Columnar organization of the characteristic ripple and phase

The responses of several cells at various depths in a given penetration were compared in order to determine if the ripple response features were columnarly organized. Figure 1 shows

examples of ripple transfer functions and response fields (RFs) of cells at different depths for three different penetration tracks. The curves obtained within a column are similar.

Data obtained from 66 cells in 23 penetrations are shown in Fig. 2, where the response curves as shown in Fig. 1 are parametrized in terms of the characteristic ripple and phase (Ω_o and Φ_o). Since Ω_o is strongly correlated to BF (see subsection on topography), the Ω_o data are shown separately for high and low BFs (with border at 4 kHz). In Fig. 2A, the left plot illustrates the distribution of Ω_o from all units in the sample (equivalent to Var_T in Eqn. (2); $\mathrm{Var}_T = 0.44$ for high-BF units). In comparison, the right plot shows the distribution of the deviation of Ω_o of each unit from the average value of its penetration (equivalent to Var_W in Eqn. (2); $\mathrm{Var}_W = 0.21$). The narrowing in columns by a factor of 0.48 ($\mathrm{Var}_W/\mathrm{Var}_T$) is significant as tests with random entries reveal a ratio of variances of 0.60-0.62. The right plot shows that 65 % of high-BF units encountered in a column are expected to be tuned to within $\pm$ 0.4 cycle/octave of the average characteristic ripple. Similar results are seen in Fig. 2B regarding the scatter of Φ_o's within a column. The percentage of units in a single penetration that lie within $\pm$ 30 degrees is 69, and the variance ratio is 0.46 (note that this includes units over the entire BF range as Φ_o does not vary with BF). In summary, it is unlikely to encounter units with drastically different RF parameters in the same penetration.

For comparison, Fig. 2 shows also the total and within-column distributions of the tonal bandwidth (BW20) and the FM directional sensitivity (C index). The BW20 of high-BF units (Fig. 2C) shows a variance ratio of 0.57, which might entirely be due to sampling errors. In other words, the bandwidth shows a columnar scatter of the order of the variation along the iso-frequency axis. The columnar distribution of index C (Fig. 2D) is similar to that of Φ_o ($\mathrm{Var}_W/\mathrm{Var}_T = 0.45$).

Correspondence between single-unit and multiunit recordings

Since all mappings of the ripple response parameters were performed with multiunit recordings, it was important to establish whether these maps reflect a similar distribution of single-unit response properties. To do so, recordings of multiunit clusters were compared to those of single units isolated from the same cluster.

In Fig. 3 the ripple transfer functions and RF's are plotted for a cluster and for two of its constituent single units. The response curves are very similar. In Fig. 4 the ripple response parameters Ω_o (A) and Φ_o (B) of each cluster are compared to the same parameters of one to three single units isolated from the same trace. For both parameters linear regression analysis indicated a weak but significant correlation ($r \approx 0.4$; $P < 0.05$) between the two types of recordings. In case of Ω_o, responses with secondary peaks in the magnitude transfer function (see example in Fig. 1C) are excluded in this analysis; in such cases the two peaks in the transfer function were usually found at similar Ω's, but the maximum could be at a different Ω, thus giving rise to a different Ω_o. Also in Fig. 4, BW20 (C) and C index (D) are compared for both single- and multiunit recordings. These parameters show a close correspondence between the two types of recordings ($r \approx 0.7$; $P < 0.001$). Note that BW20 of a cluster is, if different, mostly larger than BW20 of the constituent single neurons. Therefore, we may conclude that despite measurement errors which contribute to the scatter in the data, multiunit recordings reflect the underlying single-unit responses.

Topographic distribution of the characteristic ripple

Figure 5 shows the spatial distribution of the characteristic ripple, Ω_o, in AI for four animals. In all AI maps (Fig. 5A), closely spaced electrode penetrations were made orthogonally to the plane of the cortex and along isofrequency strips with BFs ranging from approximately 1-10 kHz.

There are two consistent trends in the distributions. The first is an overall increase in the range of Ω_o's with increasing BF. On average, the maximum Ω_o measured on a given isofrequency plane increases by a factor of about 2 as a function of BF over the range 2-10 kHz. The second trend in the Ω_o distributions occurs along the isofrequency planes where Ω_o's achieve a maximum value near the middle of AI, and decrease towards the edges. The schematic trajectory of the maximum Ω_o values is highlighted in the maps (Fig. 5A) by the dashed lines running approximately orthogonally to the isofrequency planes. In each map, there is a secondary trajectory of the Ω_o maxima that extends only partially across the BF range explored. This trend along the isofrequency lines is also demonstrated in the two-dimensional views in Fig. 5B. For all BFs Ω_o is plotted as a function of location along the axis that is parallel to the estimated isofrequency contours. For all plots, the smoothed averages (solid lines) clearly illustrate the decrease of Ω_o towards the edges. In #153, #155 and #158, the secondary maxima near the center are also well represented.

The characteristic ripple Ω_o of a multiunit cluster is correlated with the broadness of its response area (characterized by BW20), as demonstrated by the scatter plots in Fig. 6. This correlation is confirmed by the spatial distributions of the response area bandwidths (Fig. 7), which approximately resemble the Ω_o maps in Fig. 5A. To facilitate the comparison between the two sets of maps, the trajectories of the Ω_o maxima (dashed lines in Fig. 5A) are transposed to the BW20 maps. Note that in one case (#155) the bandwidth map exhibits weak evidence of a highly tuned ridge, i.e., the bandwidths seem simply to covary with BF and only little along the isofrequency planes. As in Fig. 5B the variation along the isofrequency axis is also evident in the plots of Fig. 7B; Specifically, in all plots, the smoothed curves look inverted compared to those in Fig. 5B.

Topographic distribution of the characteristic phase

The spatial distribution of the characteristic phase, Φ_o, was determined along the isofrequency planes at the same penetrations as those shown in the maps of Ω_o and BW20. The spatial distributions of Φ_o in AI are shown in Fig. 8. Responses with $|\Phi_o| > 100$ degrees are indicated with an "X" in the maps (Fig. 8A), and are excluded with respect to the shading in the map. The basic feature that emerges in the distributions is a clustering or a location dependent change in Φ_o along the isofrequency planes. Near the caudal end of AI, asymmetric RFs with negative Φ_o predominate. Towards the middle, the RFs become more symmetric ($\Phi_o \approx 0$). More rostrally, the RFs tend to be more asymmetric with a positive Φ_o. The dashed lines in each map mark schematically the region where Φ_o changes once from extreme positive to extreme negative. Beyond this region, the characteristic phase exhibits a reversal in trends. In all maps, secondary clusters of negative Φ_o can be seen near the rostral edge of AI. Responses with $|\Phi_o| > 100$ degrees tend to occur toward the edges but are not particularly clustered. There is no systematic variation with BF. Figure 8B shows the variation of Φ_o along the isofrequency direction. Except for #153, all smoothed data curves (solid lines) demonstrate a consistent dip

towards the caudal end (negative Φ_o's), and a systematic increase in Φ_o towards the rostral end.

The regression plots of Fig. 9 indicate that Φ_o is weakly but consistently correlated with the FM directional sensitivity as measured by the C index. The AI maps of the C index are presented in Fig. 10. The distributions of the C index across AI are roughly similar to those of Φ_o. To facilitate the comparison between the two sets of maps, the dashed lines in Fig. 8A are transposed to the C index maps. Note that in most maps (especially #153), there is a relative paucity of asymmetric RFs with positive Φ_o and C indices.

Joint distribution of the characteristic ripple and characteristic phase

The joint distribution of Ω_o and Φ_o is shown in the scatter plot of Fig. 11 which combines the penetrations from all maps. For all Ω_o's there is a wide range of characteristic phases, although the standard deviation in the distribution tends to decrease slightly with Ω_o.

DISCUSSION

Physiological maps of AI responses to rippled stimuli suggest that there is an orderly clustered topographic representation of the characteristic ripple and phase along the isofrequency planes. Specifically, Ω_o achieves its highest values near the middle of AI, and in some cases it forms a secondary maximum near the edges (Fig. 5). The Φ_o is near zero at the center of AI, becoming negative caudally and positive rostrally, with reversals in this trend occuring towards the edges (Fig. 8).

Since all maps illustrated in this report were constructed using multiunit records, one can at best say that the maps reflect ordered changes in neuronal activity integrated over small volumes in AI. This is because mulitunit records may in some cases average out substantial variations in single-unit responses in close proximity (Schreiner and Sutter 1992). Nevertheless, in the intermediate cortical layers III and IV, where single tones at BF evoke strong excitatory onset potentials (Shamma et al. 1993), there is a good correspondence between the characteristic ripple and phase obtained from single- and multiunit recordings (Figs. 3 and 4). This is consistent with the finding that these features remain relatively stable in single-unit recordings over a depth range of 300 μm (Figs. 1 and 2), indicating a columnar organization. Similar clustering in columns was also found for the FM directional sensitivity (C index, Fig. 2D) and for the asymmetry of the response area ($\mathrm{Var}_W/\mathrm{Var}_T = 0.42$; $N = 66$ (Shamma et al. 1993)), which is expected in view of the correlations between Φ_o, C index and asymmetry (Shamma et al. 1994).

A lack of evidence for columnar organization of BW20 (Fig. 2C) was also previously found in ferrets in our lab ($\mathrm{Var}_W/\mathrm{Var}_T = 0.64$; $N = 50$ (Vranić et al. 1993)). The columnar variability of BW20 might be due to measure errors which can occur both in determining the threshold at BF and the width of the excitatory response. If the data reflect a significant columnar variability of the response-area width, one might wonder why Ω_o while inversely correlated to BW20 (for single units: Shamma et al. 1994, for multiunit clusters: Fig. 6B) shows a columnar organization. This discrepancy might be due to nonlinearities. For instance, the bandwidth measured at a certain level, BWx (with x the level above threshold), does not fully describe the width of the excitatory response area (or tuning curve) since a large variety of tuning curves

might be found for a given BWx (cf. Schreiner and Sutter 1992). On the other hand, the RF does not vary much with overall ripple level (Shamma et al. 1994). Another explanation under assumptions of linearity would be that the bandwidth of the response area is not only related to Ω_o but also to the width of the magnitude the ripple transfer function, $|T(\Omega)|$, and to Φ_o (Shamma et al. 1994). Since Φ_o is columnarly organized one might conclude that the width of $|T(\Omega)|$ varies sufficiently within a column to disrupt uniformity of BW20.

Relation to response area asymmetry and bandwidth maps

The characteristic ripple and phase are response features defined with respect to rippled spectral stimuli. However, as demonstrated in this paper for multiunit clusters (Figs. 6 and 9), and in Shamma et al. (1994) for single units, Ω_o is correlated with the bandwidth of the response area, while Φ_o reflects approximately the asymmetry of the response area. In the multiunit recording of the asymmetry, it is assumed that the C index closely reflects the response area asymmetry (Shamma et al. 1993, 1994); the C index is an easier and somewhat more robust measure than the true asymmetry measure (e.g., it does not require exact BF measurements), and was therefore used in the mappings (Fig. 10). Both of the response area measures have been extensively mapped earlier (bandwidth: Schreiner and Mendelson (1990) and Heil et al. (1992a); asymmetry: Shamma et al. (1993)) and have shown similar distribution patterns to those of Ω_o and Φ_o. This finding lends further support to the argument that rippled spectra and tonal stimuli generate largely equivalent representations of cell responses in AI, and that therefore there is a substantial linear component in the responses in the sense discussed in Shamma et al. (1994).

Several cells had a characteristic phase which corresponds to an inverted response field ($|\Phi_o| \approx 180$), i.e., with a centered inhibitory response and two excitatory sidebands. These responses seem to be associated with the multipeaked response areas as reported for cat AI by Sutter and Schreiner (1991). However, in contrast to their findings, inverted RFs did not appear clustered in a specific AI region in the ferret.

The origin of the Ω_o and Φ_o organization is uncertain since no maps of rippled spectral responses have been previously reported in pre-cortical structures. However, certain trends might be related to pre- cortical origins. For instance, the overall increase of Ω_o with increasing BF (Fig. 5A) is likely related to the progressively sharper tuning of the cochlear filters with higher BF (e.g. Kiang et al. 1965; Evans 1972).

Functional interpretation of rippled spectral maps

Parametrizing and mapping responses in terms of characteristic ripple phase Φ_o and frequency Ω_o have two equivalent interpretations for the functional organization of AI. The first arises from the correspondence of these measures to the response area asymmetry and bandwidth. The Φ_o map can be thought of as implicitly encoding the local gradient of the spectral profile since that is the intuitive interpretation of response area asymmetry (Shamma et al. 1993). Similarly, the Ω_o map is implicitly assumed to detect the bandwidth of the input spectral profile (Schreiner and Mendelson 1990).

The second more abstract view is to consider each cortical cell to be a "ripple filter" tuned to a particular ripple frequency (Ω_o) and phase (Φ_o). By having a bank of these filters tuned to different Ω_o's and Φ_o's, AI can analyze an input spectral profile into different channels along two new independent axes: the ripple magnitude and phase. Since AI cells respond relatively locally

around their BF, the ripple analysis is local in nature, and hence the tonotopic axis remains an important third organizational axis. The spectral-ripple representation is analogous to that produced by the cochlear filters for tones. The analogy is exact if the spectral profile against the tonotopic axis is thought of as the sound waveform against the time axis. The cortex then performs an analysis on the input spectral pattern and spreads it out along the Ω_o (analogous to the spatial axis of the cochlea) and the Φ_o axis (analogous to the phase of the synchronous responses in the auditory nerve).

This type of analysis is also thought to operate in the primary visual cortex (VI) (De Valois and De Valois 1988). There, spectral ripples are replaced by two dimensional sinsoidal gratings of different spatial frequencies. Using such images as stimuli, the anatomical, physiological, and psychophysical data are shown to be consistent with the notion that different spatial frequencies are orderly mapped across VI. The fundamental difference between the AI and VI maps is that the latter are two dimensional. Each cell in VI is tuned to a specific pair of characteristic spatial frequencies (e.g., Ω_o^x and Ω_o^y along the horizontal and vertical axes, respectively). Implied in such a tuning is an orientation selectivity and its orderly mapping since the orientation of any grating can be equivalently defined in terms of a specific pair of ripples (Ω_o^x, Ω_o^y). Also, simple cells in VI are sensitive to the phase of the sinusoidal gratings. However, there are no reports known on mappings of the phase axis in VI, and hence it is unknown if the Φ_o maps seen in AI also exist in VI.

There are several benefits of a ripple representation for spectral profiles. One is the efficiency of the resulting code since spectral profiles, just as images (De Valois and De Valois 1988), tend to incorporate overall periodic patterns that can be sufficiently captured by a few Fourier coefficients. Another important benefit is that a repeated representation of the profile is available at various scales or levels of detail. That is, cells tuned to low Ω_o's extract a heavily smoothed version of the profile, and those tuned to high Ω_o's capture the fine details of the profile. Once a range of these representations is available, postprocessing of the profile becomes relatively easy. For instance, a spectral profile can be stablized with respect to relatively slow spectral distortions such as pre-emphasis or lowpass filtering by simply suppressing its lower Ω's. Or, it may be smoothed by suppressing the higher Ω's in order to remove the effects of very sharp spectral notches and peaks such as those introduced by the pinna (Blauert 1983).

Relating ripple analysis to the physiological maps

For the theoretical framework outlined above to be operative in AI, it is essential that a full mapping of the Ω_o and Φ_o axes are available. That is, at each BF, a full range of Ω_o's must be represented; and at each Ω_o, all Φ_o values should exist. The maps shown in Figs. 5 and 8 for the most part satisfy these requirements. The requirements are not met with respect to the dependence of the distributions on BF. Specifically, only small Ω_o's (< 1 cycle/oct) are represented at low BFs (Fig. 5A). This suggests that an input spectral profile is only relatively coarsely encoded at its lower BF portions. One implication of this finding would be that the higher harmonics of a sound complex cannot be resolved in the ferret AI, as seems also to be the case in the cat (Calhoun and Schreiner 1993). We do not exclude, however, that a higher range of Ω_o's exist in other species (as in monkey, Schwarz and Tomlinson 1990), especially at lower BFs, making the harmonic representation possible. It is also possible that fine encoding of a spectral profile is established by a phase-insensitive response tuned to high Ωs. Some cells in ferret AI showed (apart from AC tuning to low Ωs) a DC tuning to high Ωs (Shamma et al.

1994).

There is another topological difficulty arising from the maps concerning the question of how three axes (BF, Ω_o, and Φ_o) can be effectively mapped upon a two dimensional AI surface. Thus, while at each BF a certain range of characteristic ripples and phases are represented along the isofrequency plane, the two parameters are nevertheless not fully represented with respect to each other. Instead, both the Ω_o and Φ_o axes run orthogonally to the isofrequency planes, and hence a specific Ω_o can effectively intersect only one or two Φ_o values. This situation is even harder to visualize in the visual system, where 6 axes presumably co-exist.

In general, this difficulty can be resolved in two ways. The first is that a finer mapping of these parameters exists, one that is not detectable in the relatively coarse sampling used in our experiments. With such a scheme, it is possible that the characteristic ripple and phase are micro-mapped relative to each other around each location in AI. The other possibility is that the two parameters are mapped relative to each other more than once, each time at a different parameter range. This would be for instance the purpose of the second peak in the Ω_o maps (Fig. 5) and the reversals in the Φ_o maps (Fig. 8). It is also possible that an additional field, such as the AAF with its significantly broader bandwidths (lower Ω_o's), may provide the repeated mappings (Kowalski et al. 1993).

ACKNOWLEDGEMENTS

This work is supported by grants from the Air Force Office of Scientific Research, and from the Office of Naval Research. We would like to thank P. Gopalaswamy for his help in developing the data acquisition system, K. Wang for his contribution to the analysis of the ripple responses, and A.L. Owens for his assistance in surgery and data recordings. The authors are members of the Institute for Systems Research which is partially funded by an NSF grant (# NSFD CD 8803012).

REFERENCES

BLAUERT, J. *Spatial hearing: the psychoacoustics of human sound localization.* Cambridge: M.I.T. Press, 1983.

CALHOUN, B. M. AND SCHREINER, C. E. Spatial frequency filters in cat auditory cortex (Abstract). *Soc. Neurosci.*, Washington, D.C., 1993.

DE VALOIS, R. AND DE VALOIS, K. *Spatial Vision.* New York: Oxford University Press, 1988.

DUDA, R. O. AND HART, P. E. *Pattern classification and scene analysis.* New York: J. Wiley & Sons, 1973.

EVANS, E. F. The frequency response and other properties in guinea pig cochlear nerve. *J. Physiol.* 226: 263-287, 1972.

HEIL, P., RAJAN, R. AND IRVINE, D. Sensitivity of neurons in cat primary auditory cortex to tones and frequency-modulated stimuli. II. Organization of response properties along the iso-frequency dimension. *Hear. Res.* 63: 135-156, 1992.

KIANG, N. Y. S., WATANABE, T., THOMAS, E. C. AND CLARK, L. F. *Discharge patterns of single fibers in the cat's auditory nerve.* M.I.T. Research Monograph No.35, Cambridge: M.I.T. Press, 1965.

KOWALSKI, N., VERSNEL, H. AND SHAMMA, S. A. Characteristics of an anterior field in the ferret auditory cortex (Abstract). *Assoc. Res. Otolaryngol. 16*, St. Petersburg Beach, Florida, 1993.

MENDELSON, J. R., SCHREINER, C. E., SUTTER, M. L. AND GRASSE, K. L. Functional topography of cat primary auditory cortex: responses to frequency-modulated sweeps. *Exp. Brain. Res.* 94: 65-87, 1993.

MERZENICH, M. M., KNIGHT, P. L. AND ROTH, G. L. Representation of cochlea within primary auditory cortex in the cat. *J. Neurophysiol.* 28: 231-249, 1975.

MIDDLEBROOKS, J. C., DYKES, R. W. AND MERZENICH, M. M. Binaural response-specific bands in primary auditory cortex (AI) of the cat: Topographical organization orthogonal to isofrequency contours. *Brain Res.* 181: 31-48, 1980.

PHILLIPS, D. P., ORMAND, S. S., MUSICANT, A. D. AND WILSON, G. F. Neurons in the cat's primary auditory cortex distinguished by their responses to tones and wide-spectrum noise. *Hear. Res.* 18: 73-86, 1985.

PHILLIPS, D. P., SEMPLE, M. N., CALFORD, M. B. AND KITZES, L. M. Representation of tonal stimuli in cat primary auditory cortex: dependence on stimulus level (Abstract). *Assoc. Res. Otolaryngol. 16*, St. Petersburg Beach, Florida, 1993.

SCHREINER, C. E. AND MENDELSON, J. R. Functional topography of cat primary auditory cortex: distribution of integrated excitation. *J. Neurophysiol.* 64: 1442-1459, 1990.

SCHREINER, C. E. AND SUTTER, M. L. Topography of excitatory bandwidth in cat primary auditory cortex: single-neuron versus multiple-neuron recordings. *J. Neurophysiol.* 68: 1487-1502, 1992.

SCHWARZ, D. W. AND TOMLINSON, R. W. Spectral response patterns of auditory cortical neurons to harmonic complex tones in alert monkey (Macaca mulatta). *J. Neurophysiol.* 64: 282-297, 1990.

SHAMMA, S. A., FLESHMAN, J. W., WISER, P. R. AND VERSNEL, H. Organization of response areas in ferret primary auditory cortex. *J. Neurophysiol.* 69: 367-383, 1993.

SHAMMA, S. A., VERSNEL, H. AND KOWALSKI, N. Ripple analysis in the ferret primary auditory cortex. I. Response characteristics of single units to sinusoidally rippled spectra. *ISR Technical Report 94-20, University of Maryland, College Park,* 1994.

SUGA, N. The extent to which biosonar information is presented in the bat auditory cortex. In: *Dynamic aspects of neocortical function* edited by G. M. Edelman, W. E. Gall and W. M. Cowan. New York: Wiley, 1984, p. 315-337.

SUTTER, M. L. AND SCHREINER, C. E. Physiology and topography of neurons with multipeaked tuning curves in cat primary auditory cortex. *J. Neurophysiol.* 65: 1207-1226, 1991.

VRANIC´, S., VERSNEL, H. AND SHAMMA, S. A. Single and double spectral peaks: psychoacoustical and physiological results (Abstract). *Assoc. Res. Otolaryngol. 16*, St. Petersburg Beach, Florida, 1993.

Figure Legends

FIG. 1. Examples of ripple transfer functions and response fields (RFs) of cells at different depths for three separate penetration tracks (*A*, *B* and *C*). For each cell the magnitude of its transfer function $|T(\Omega)|$ is shown in the left plot. The solid lines in these plots represent smoothed lines connecting the data points (smoothing performed by linearly interpolating the slopes between the midpoints of adjacent segments). The RFs are shown in the plots on the right.

FIG. 2. Distribution histograms for single units of their characteristic ripple Ω_o (*A*), characteristic ripple phase, Φ_o (*B*), the tonal bandwidth BW20 (*C*), and index *C* of the FM directional sensitivity (*D*). The parameters are computed for 23 penetrations in 7 animals. For each parameter the left plot shows the total distribution. The right plot shows the average distribution per cortical column, i.e., the deviation of the parameter value of a cell from the average value within the its column. For Ω_o and BW20 the values for low and high BF are indicated separately because of the significant dependence on BF for these two parameters.

FIG. 3. Ripple responses from a cluster (*A*) and two of constituent single units (*B* and *C*) in comparison. For the cluster and both units, the left plot depicts the magnitude of its ripple transfer function $|T(\Omega)|$. The solid lines represent smoothed lines connecting the data points (as in Fig. 1). The center plot shows the phase function $\Phi(\Omega)$, with the solid line representing the linear fit to the data points. The right plot illustrates the corresponding RF. Parameters Ω_o, Φ_o and BF_{RF}, indicated in the plots left to right respectively, are very similar for cluster and units.

FIG. 4. Parameter values derived from single-unit recordings versus parameter values from multi-unit cluster responses recorded at the same location in the cortex. The solid lines represent the y=x lines with y for the single-unit recorded value and x for the multiunit recorded value. Correlation coefficients according to linear regression analysis are indicated in the left-hand corner of each plot. *A*: Characteristic ripple Ω_o. Here the responses with a double peak in the magnitude transfer function $|T(\Omega)|$ are indicated seperately (squares or triangles) from the single-peak responses (circles). In cases of two peaks the maximum for the cluster might be at the lower Ω and for the corresponding unit at the higher Ω, or vice versa, whereas the peaks are at similar Ω values. For the single-peak responses the correlation between multiunit and single-unit values is significant ($r = 0.45$; $P < 0.05$). *B*: Characteristic ripple phase, Φ_o. *C*: The tonal bandwidth BW20. *D*: Index *C* of the FM directional sensitivity.

FIG. 5. *A*: Maps of distribution of Ω_o in AI for experiments #153, #154, #155, and #158. The scaling bar on the left indicates the values represented by the grey intensities. A Gaussian weighted filling was applied to obtain the values between penetration locations. Original values at the electrode locations were preserved. The map is made on the basis of responses where $|\Phi_o| \leq 100^o$. The small circles mark the locations for these responses. The dashed lines connect local maxima of Ω_o. Note secondary trajectories of local maxima. The solid lines indicate the isofrequency contours. Interpolation of these contours was performed with a kernel smoothing. *B*: Scatterplots of Ω_o versus location X along the isofrequency axis corresponding to the maps of *A*. The choice of the orientation of X is indicated by the arrow near the plot. The same

recordings are used as in the maps. The solid lines represent smoothed moving-window averages of the data (50 μm rectangular window at 25 μm intervals of X).

FIG. 6. Scatterplots of ripple-response parameter Ω_o versus tonal response parameter BW20 for the same four experiments as shown in Fig. 5.

FIG. 7. *A*: Maps of cortical distribution of BW20. See Fig. 5*A* for explanation of grey scaling and isofrequency contours. The schematic trajectories of maxima of Ω_o are shown to facilitate the comparison between the spatial distributions of Ω_o (Fig. 5*A*) and BW20. *B*: Scatterplots of BW20 versus location X along the isofrequency axis. The solid lines represent smoothed moving-window averages of the data (50 μm rectangular window at 25 μm intervals of X).

FIG. 8. *A*: Maps of cortical distribution of Φ_o for experiments #153, #154, #155, and #158. Grey scale representation and isofrequency contours as in Fig. 5*A*. Responses with $|\Phi_o| > 100$ degrees are excluded from the grey scaling, the locations of these responses are indicated with "X" marks. The dashed lines represent the contours of maxima and minima of Φ_o ("ridges" and "valleys", respectively), reflecting the extrema of asymmetric responses. *B*: Scatterplots of Φ_o versus location X along the isofrequency axis. The solid lines represent smoothed moving-window averages of the data (50 μm rectangular window at 25 μm intervals of X).

FIG. 9. *A*: Scatterplots of ripple-response parameter Φ_o versus FM directional sensitivity (*C* index) for the same four experiments as described in Fig. 7.

FIG. 10. *A*: AI Maps of FM directional sensitivity (*C* index). See Fig. 5*A* for legend on grey scaling and isofrequency contours. The schematic contours of maxima and minima of of Φ_o are shown to facilitate the comparison between the spatial distributions of Φ_o (Fig. 7*A*) and index *C*. *B*: Scatterplots of *C* index versus location X along the isofrequency axis. The solid lines represent smoothed moving-window averages of the data (50 μm rectangular window at 25 μm intervals of X).

FIG. 11. Joint distribution of Ω_o and Φ_o for all data from experiments #153, #154, #155, and #158. The means and SD of Φ_o were computed at eight windows of Ω_o (0-0.3; 0-0.4; 0.3-0.6; 0.4-0.8; 0.6-1.2; 0.8-1.6; 1.2-2.4; 1.6-3.2); the dashed lines represent a smoothed connection of the 2SD edges.

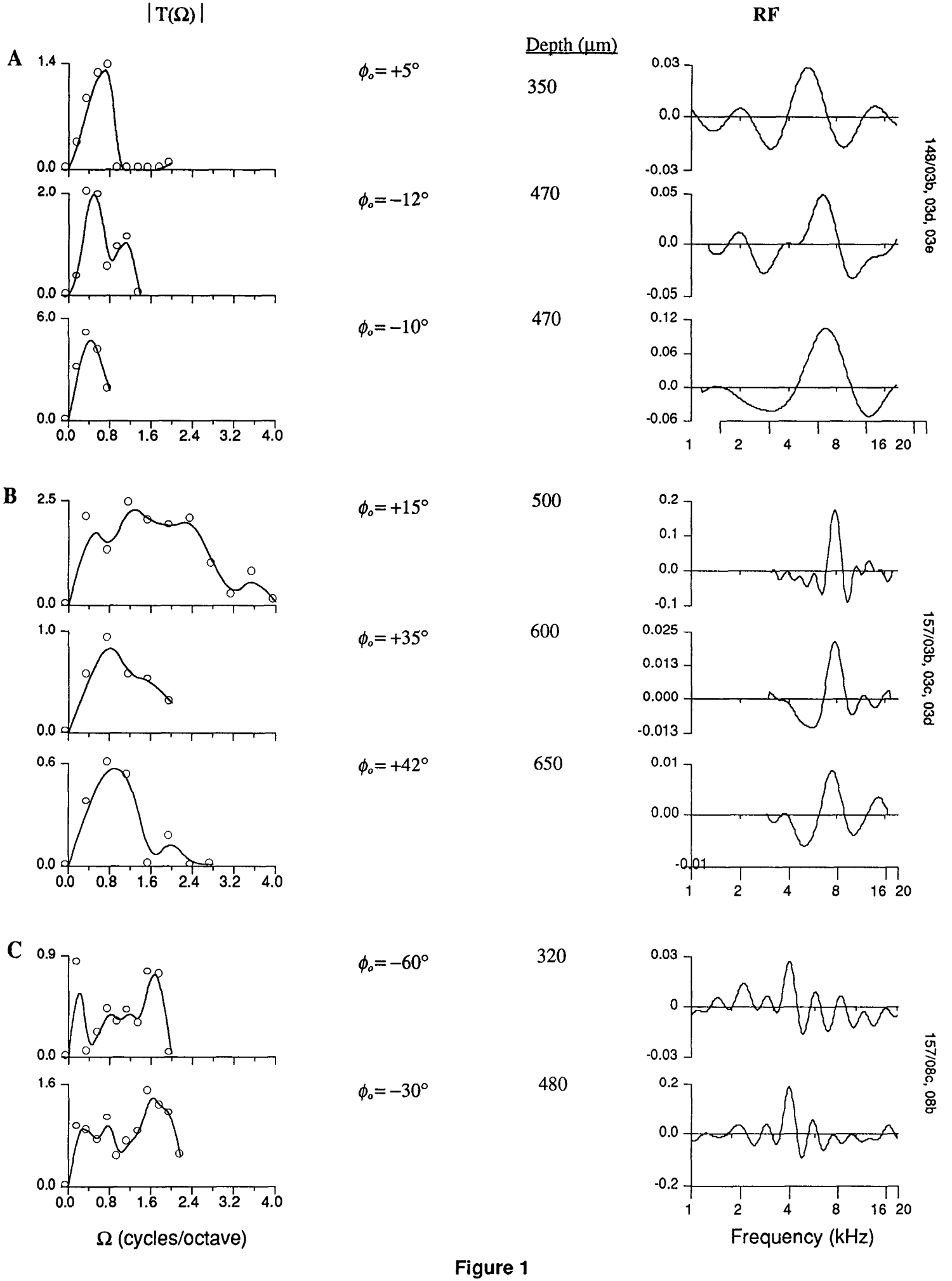
|T(Ω)|
RF
Depth (μm)
A
B
C
φo = +5°
φo = −12°
φo = −10°
φo = +15°
φo = +35°
φo = +42°
φo = −60°
φo = −30°
350
470
470
500
600
650
320
480
148/03b, 03d, 03e
157/03b, 03c, 03d
157/08c, 08b
Ω (cycles/octave)
Frequency (kHz)

Figure 1

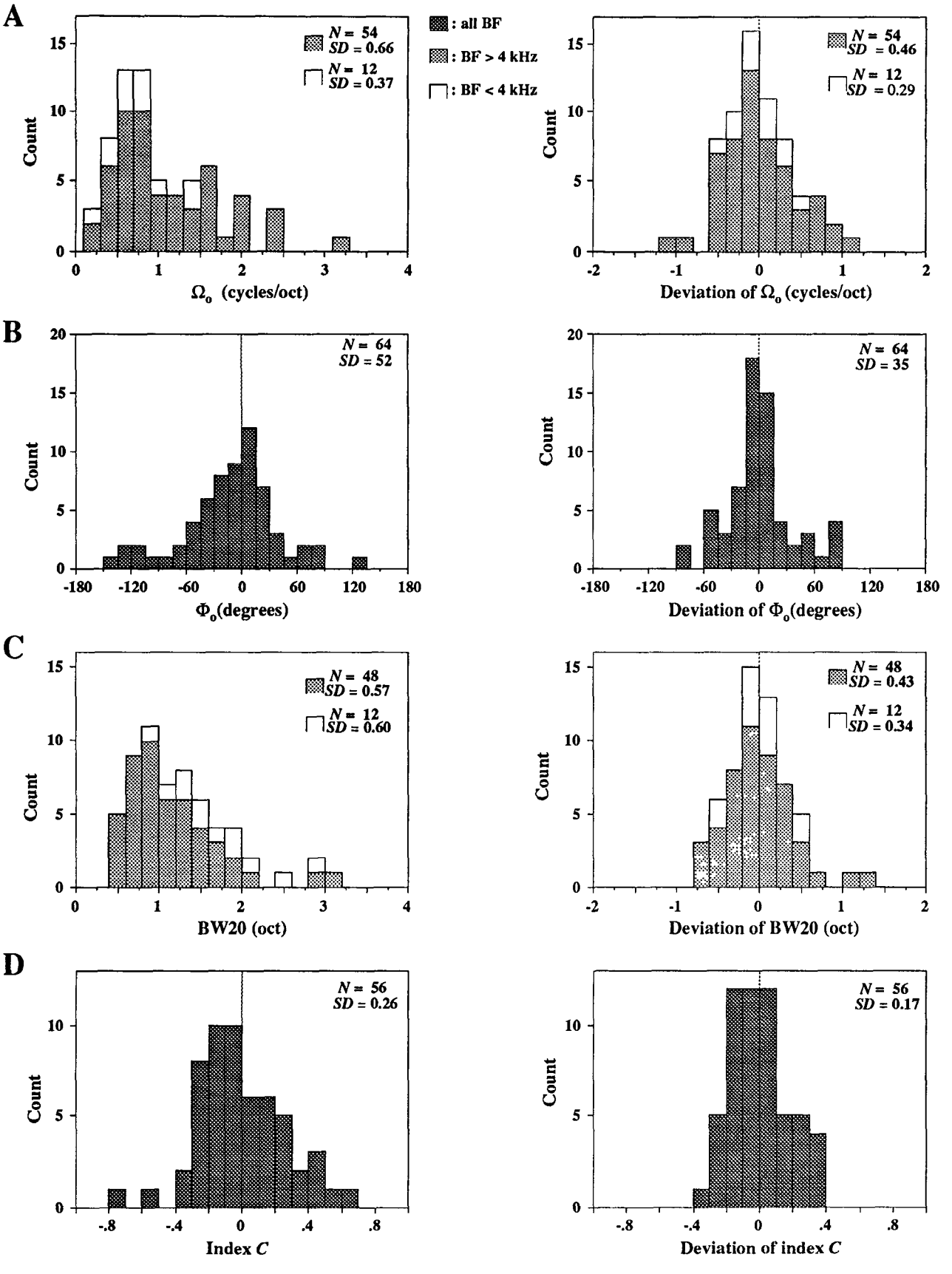
A
: all BF
: BF > 4 kHz
: BF < 4 kHz
N = 54
SD = 0.66
N = 12
SD = 0.37
Count
Ω0 (cycles/oct)
N = 54
SD = 0.46
N = 12
SD = 0.29
Deviation of Ω0 (cycles/oct)
B
N = 64
SD = 52
Φ0(degrees)
N = 64
SD = 35
Deviation of Φ0(degrees)
C
N = 48
SD = 0.57
N = 12
SD = 0.60
BW20 (oct)
N = 48
SD = 0.43
N = 12
SD = 0.34
Deviation of BW20 (oct)
D
N = 56
SD = 0.26
Index C
N = 56
SD = 0.17
Deviation of index C

Figure 2

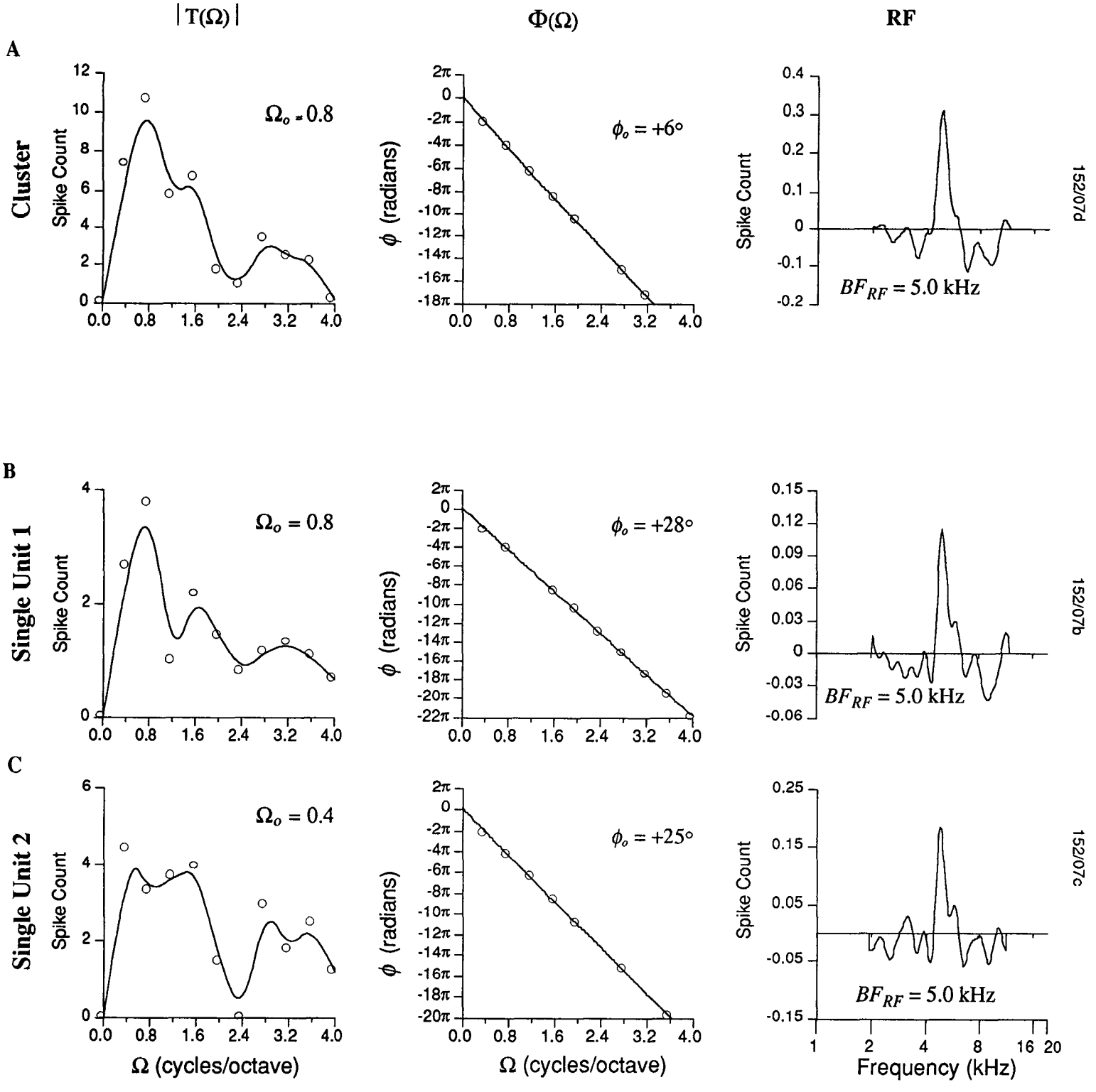
|T(Ω)|
Φ(Ω)
RF
A
Cluster
Spike Count
Ω_o = 0.8
φ (radians)
φ_o = +6°
Spike Count
BF_RF = 5.0 kHz
152/07d
B
Single Unit 1
Spike Count
Ω_o = 0.8
φ (radians)
φ_o = +28°
Spike Count
BF_RF = 5.0 kHz
152/07b
C
Single Unit 2
Spike Count
Ω_o = 0.4
φ (radians)
φ_o = +25°
Spike Count
BF_RF = 5.0 kHz
152/07c
Ω (cycles/octave)
Ω (cycles/octave)
Frequency (kHz)

Figure 3

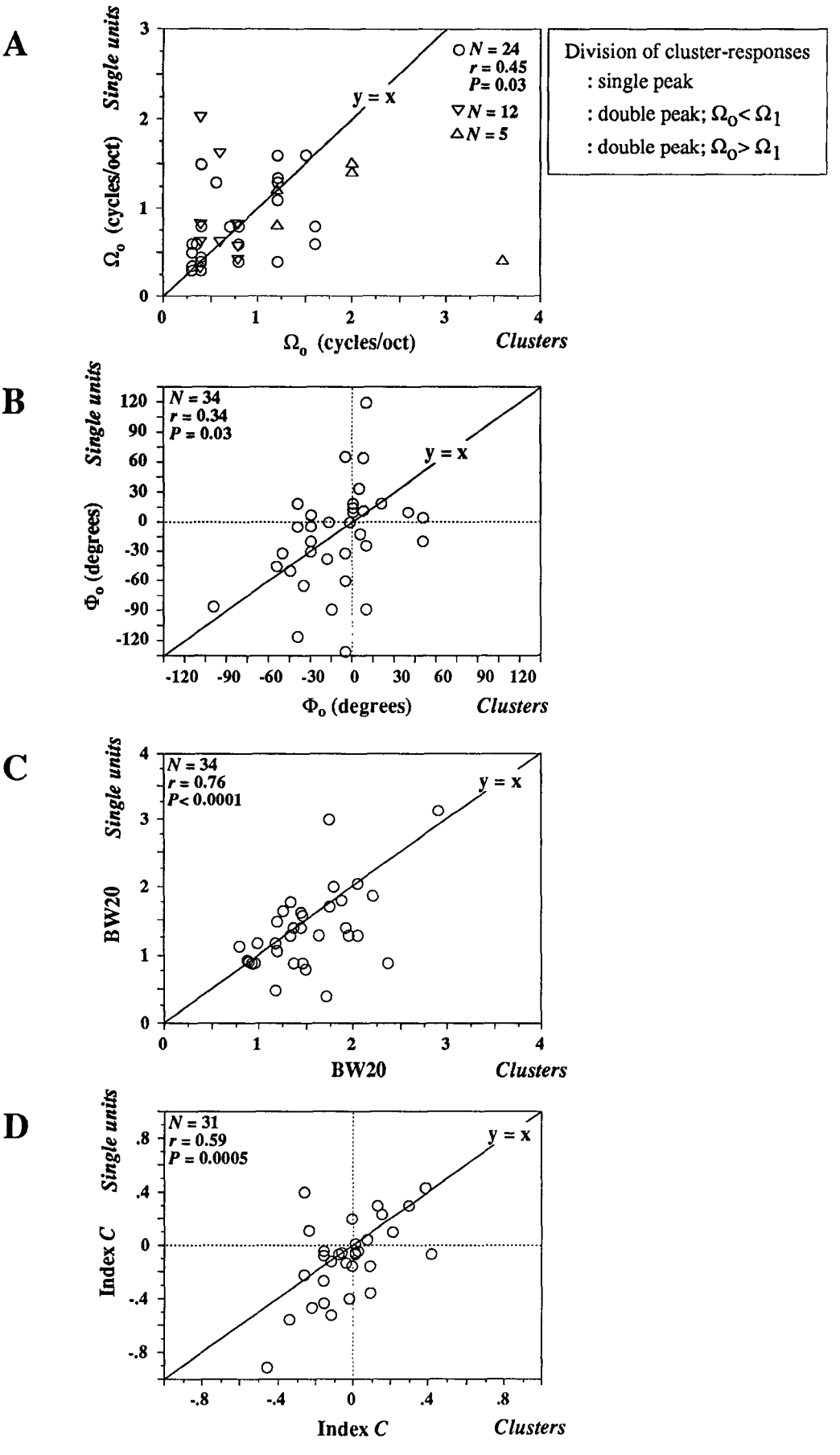
A
B
C
D
Single units
Clusters
y = x
N = 24
r = 0.45
P= 0.03
N = 12
N = 5
Division of cluster-responses
: single peak
: double peak; Ω0< Ω1
: double peak; Ω0> Ω1
Ω0 (cycles/oct)
N = 34
r = 0.34
P = 0.03
Φ0 (degrees)
N = 34
r = 0.76
P< 0.0001
BW20
N = 31
r = 0.59
P = 0.0005
Index C

Figure 4

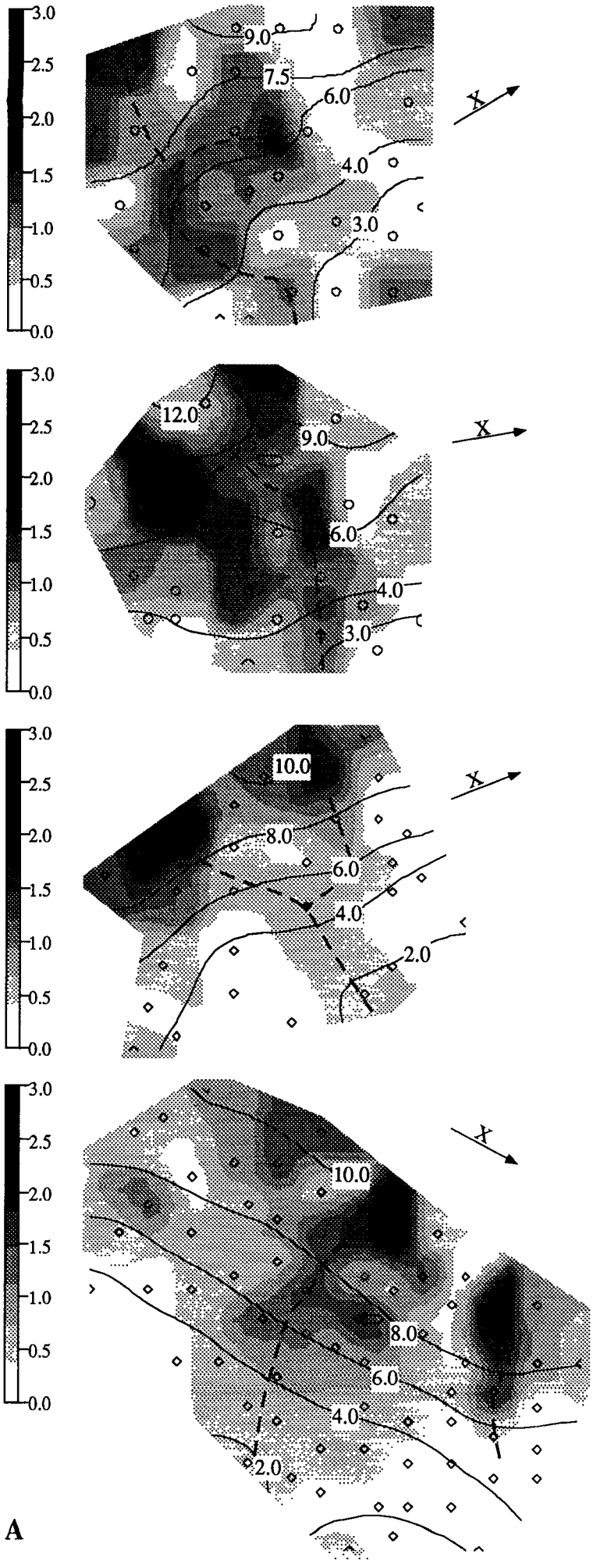
3.0
2.5
2.0
1.5
1.0
0.5
0.0
9.0
7.5
6.0
4.0
3.0
X
12.0
9.0
6.0
4.0
3.0
X
10.0
8.0
6.0
4.0
2.0
X
10.0
8.0
6.0
4.0
2.0
X

A

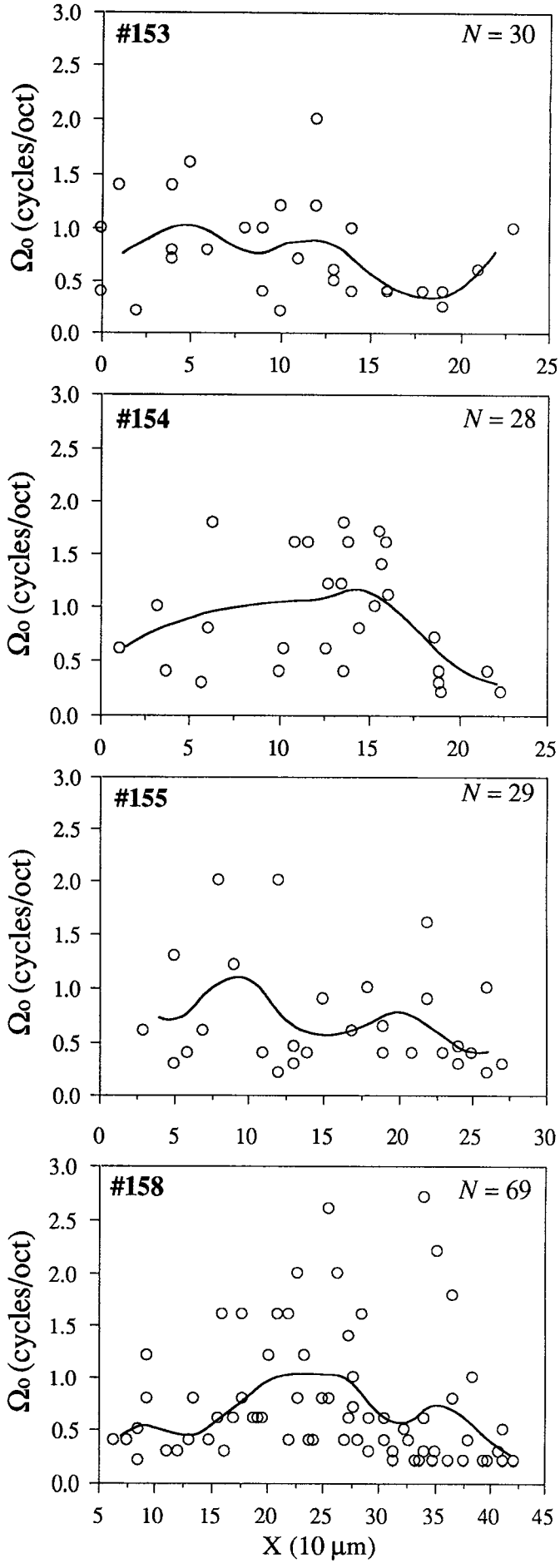
#153
N = 30
#154
N = 28
#155
N = 29
#158
N = 69
Ωo (cycles/oct)
X (10 μm)

B

Figure 5

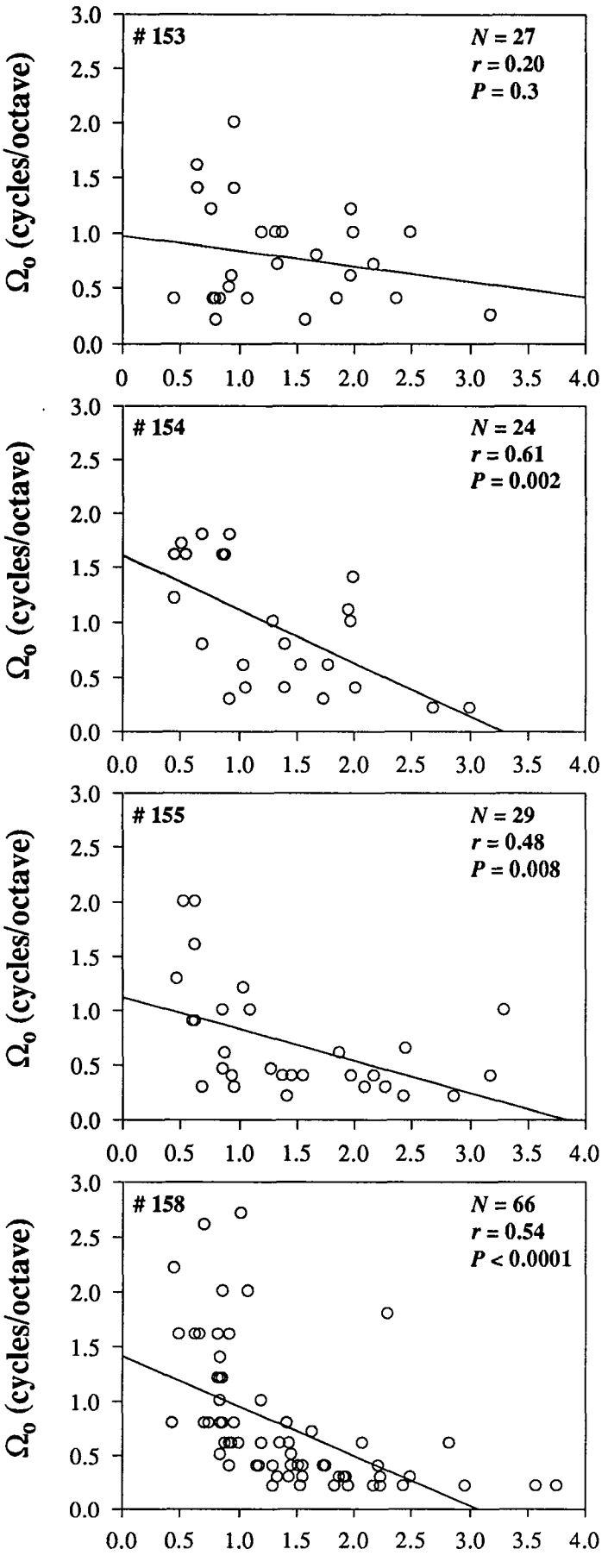
# 153
N = 27
r = 0.20
P = 0.3
# 154
N = 24
r = 0.61
P = 0.002
# 155
N = 29
r = 0.48
P = 0.008
# 158
N = 66
r = 0.54
P < 0.0001
Ωo (cycles/octave)
BW20 (octaves)

Figure 6

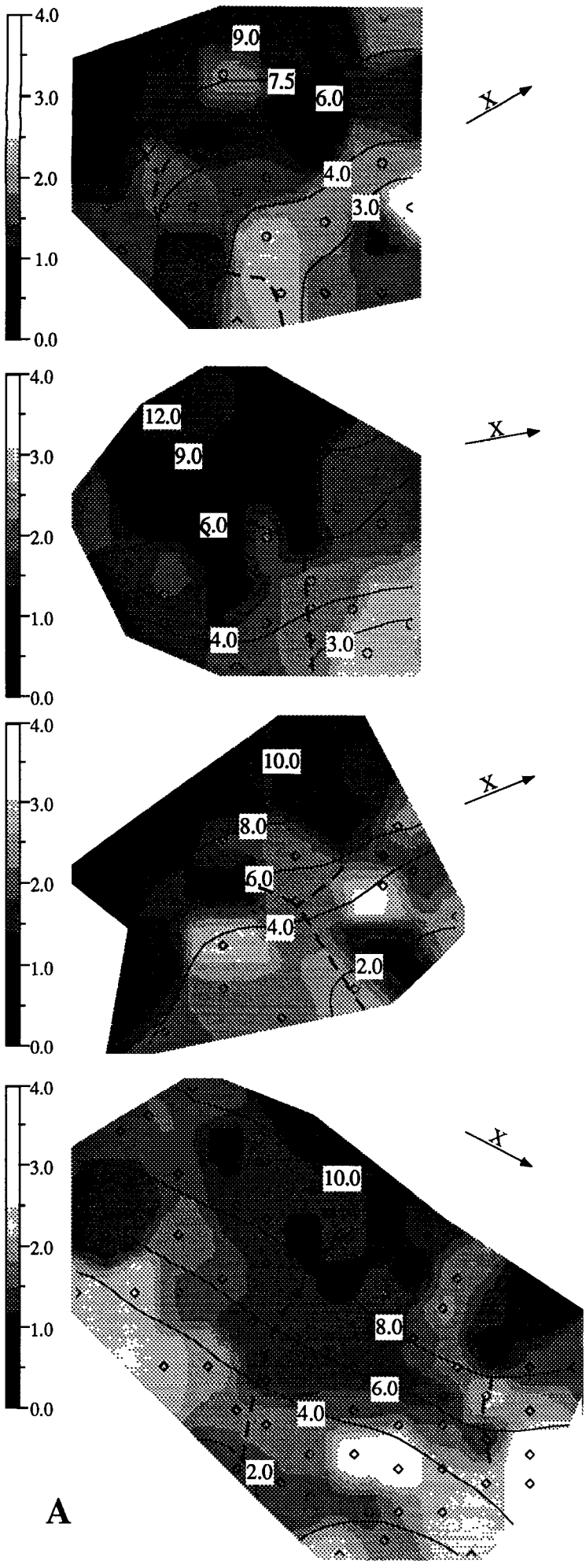
9.0
7.5
6.0
4.0
3.0
12.0
9.0
6.0
4.0
3.0
10.0
8.0
6.0
4.0
2.0
10.0
8.0
6.0
4.0
2.0
X
4.0
3.0
2.0
1.0
0.0

A

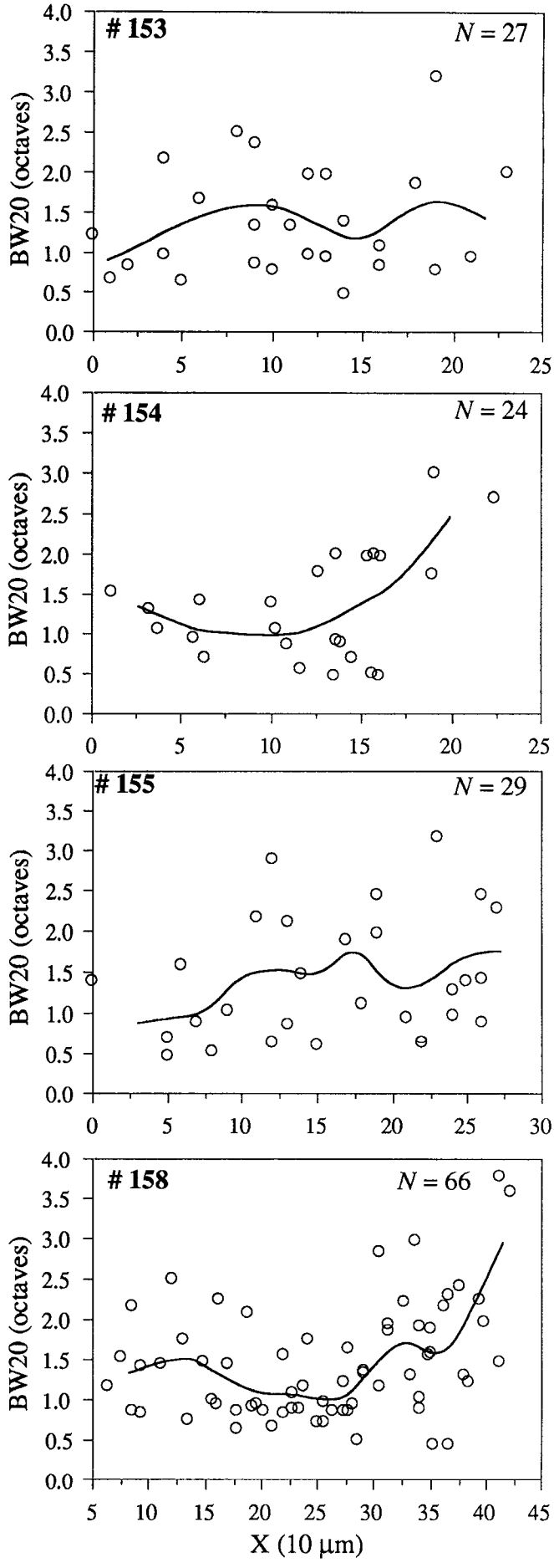
# 153
N = 27
# 154
N = 24
# 155
N = 29
# 158
N = 66
BW20 (octaves)
X (10 μm)

B

Figure 7

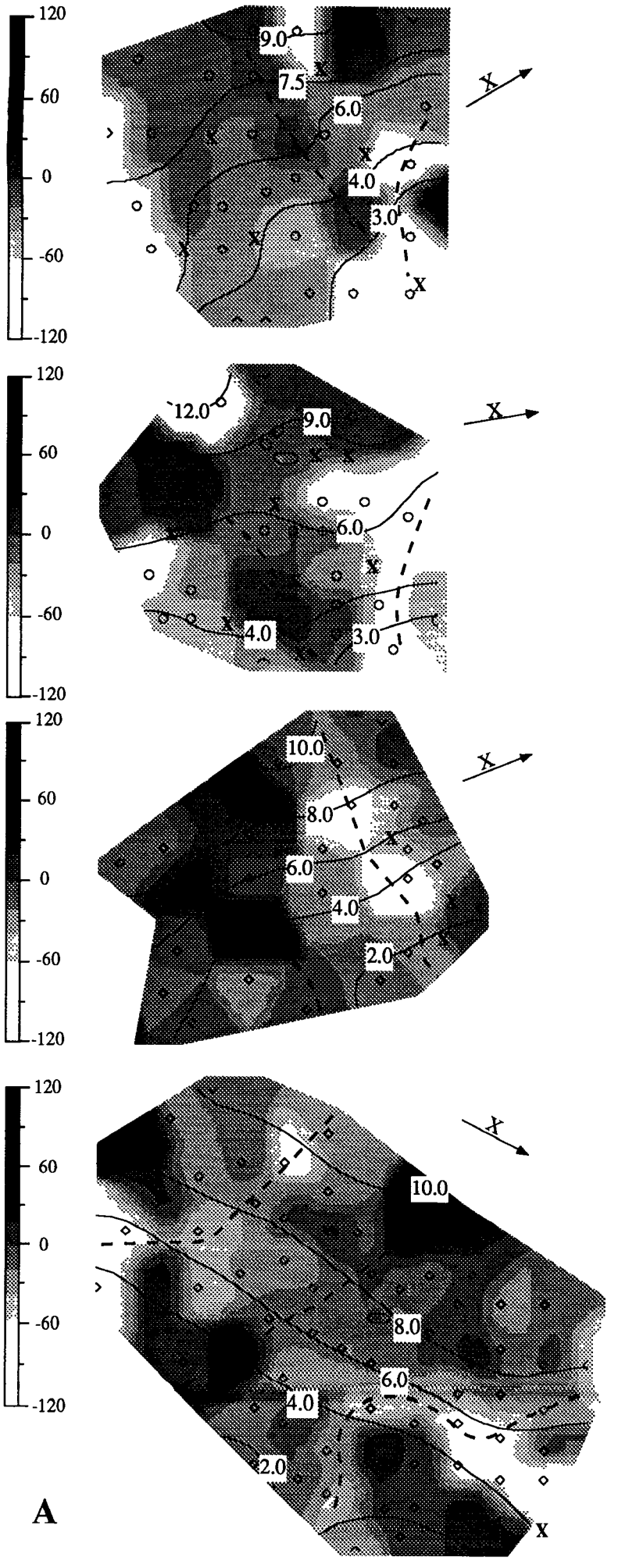
120
60
0
-60
-120
9.0
7.5
6.0
4.0
3.0
X
12.0
9.0
6.0
4.0
3.0
10.0
8.0
6.0
4.0
2.0
10.0
8.0
6.0
4.0
2.0
A

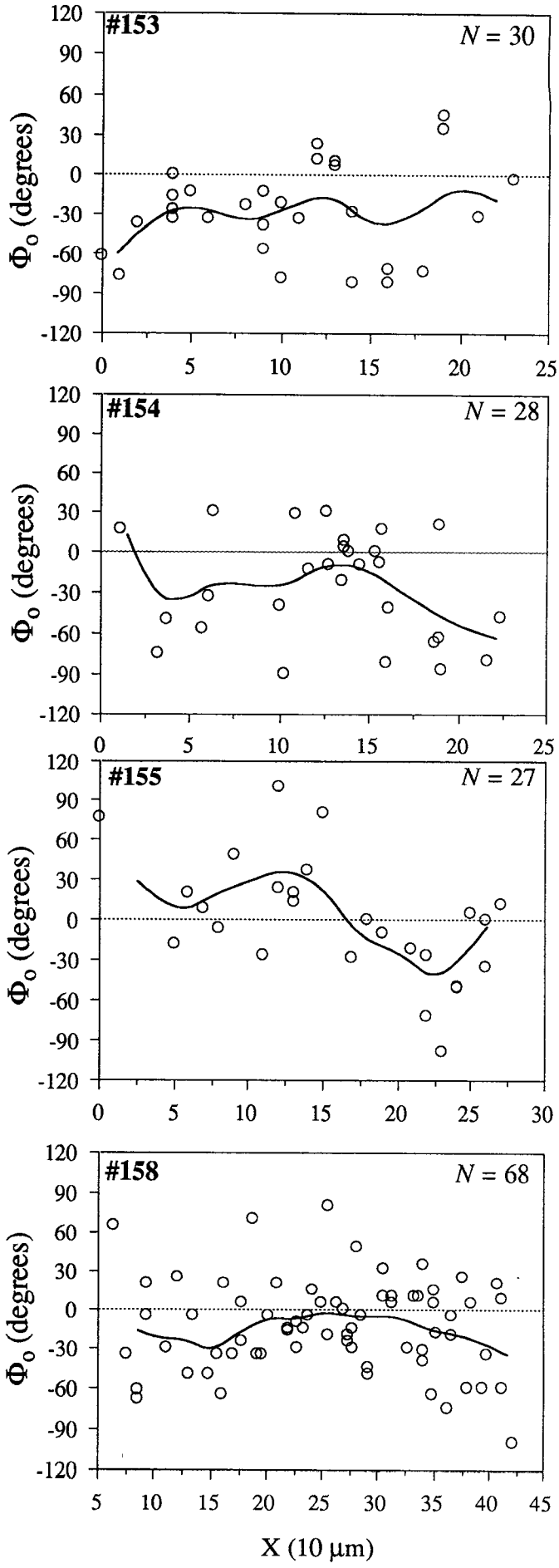
#153
N = 30
#154
N = 28
#155
N = 27
#158
N = 68
Φo (degrees)
X (10 μm)
B

Figure 8

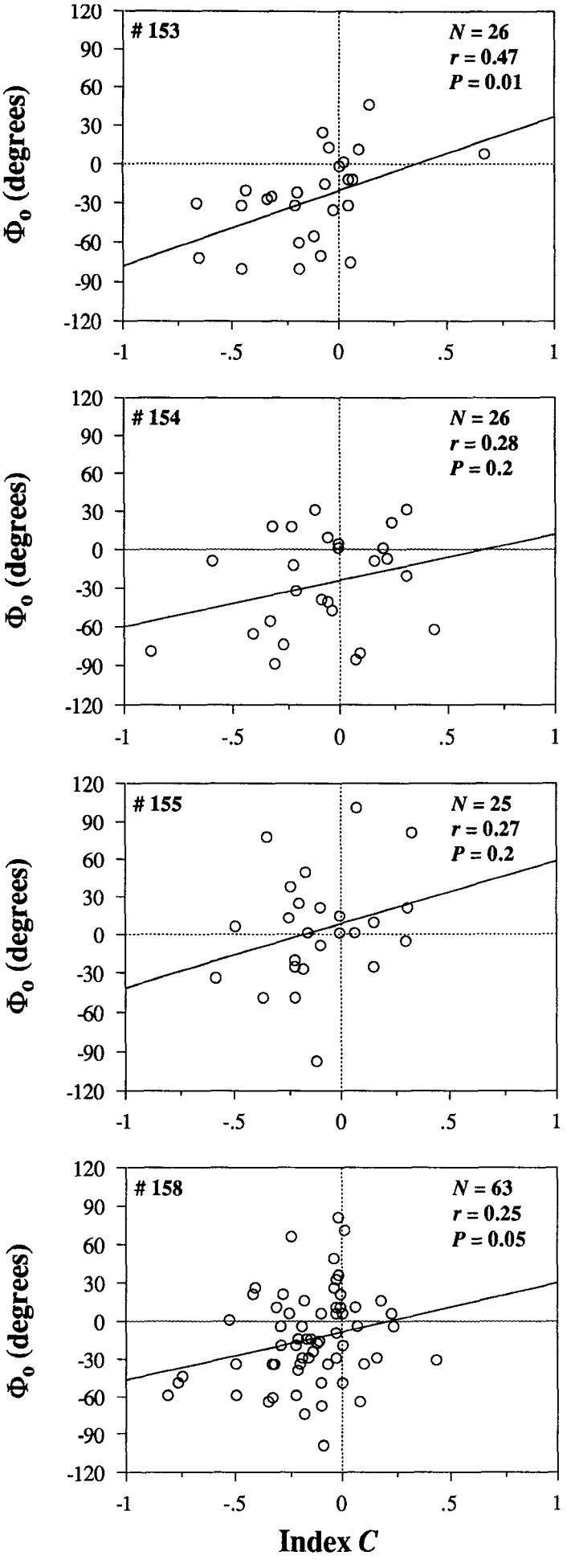
# 153
N = 26
r = 0.47
P = 0.01
# 154
N = 26
r = 0.28
P = 0.2
# 155
N = 25
r = 0.27
P = 0.2
# 158
N = 63
r = 0.25
P = 0.05
Φo (degrees)
120
90
60
30
0
-30
-60
-90
-120
-1
-.5
0
.5
1
Index C

Figure 9

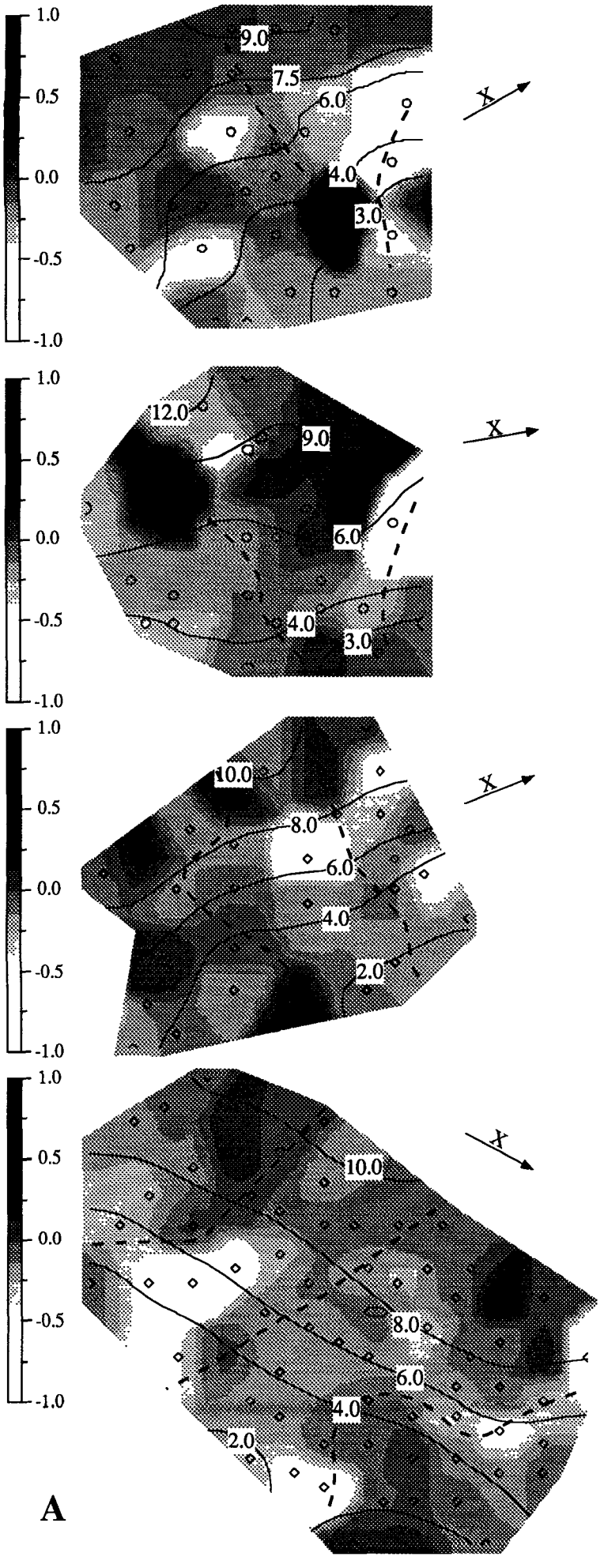
1.0
0.5
0.0
-0.5
-1.0
9.0
7.5
6.0
4.0
3.0
X
12.0
9.0
6.0
4.0
3.0
X
10.0
8.0
6.0
4.0
2.0
X
10.0
8.0
6.0
4.0
2.0
X
A

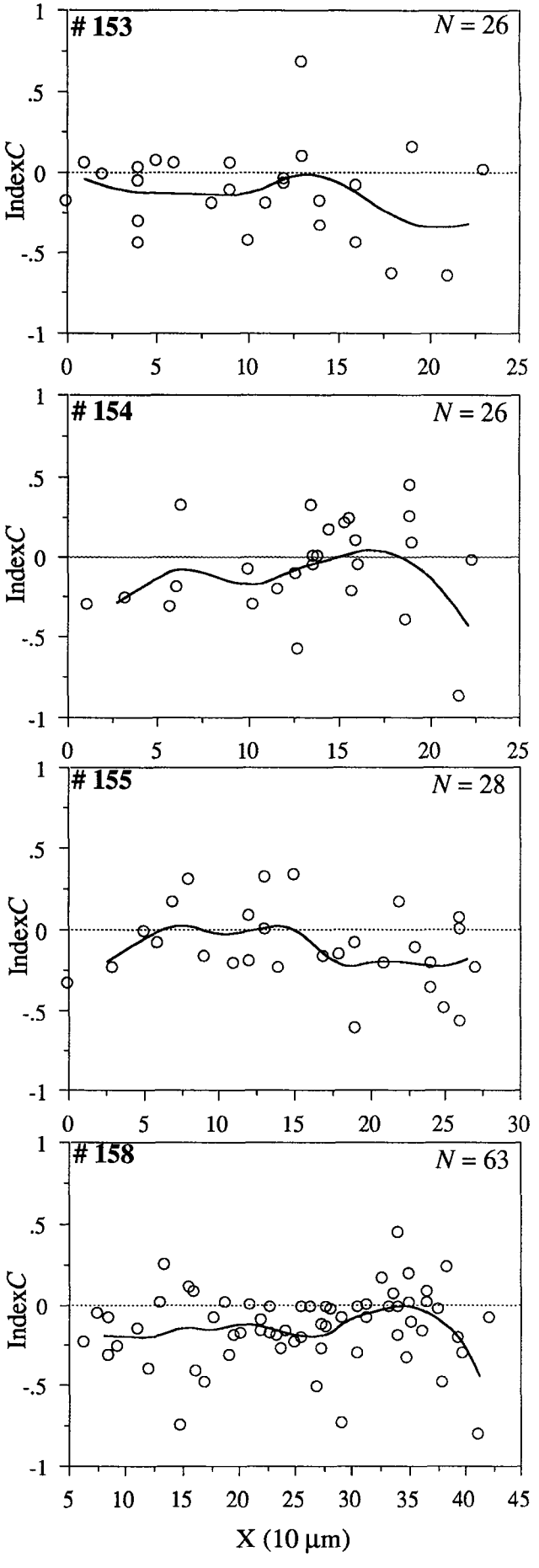
# 153
N = 26
# 154
N = 26
# 155
N = 28
# 158
N = 63
IndexC
1
.5
0
-.5
-1
0
5
10
15
20
25
30
35
40
45
X (10 µm)
B

Figure 10

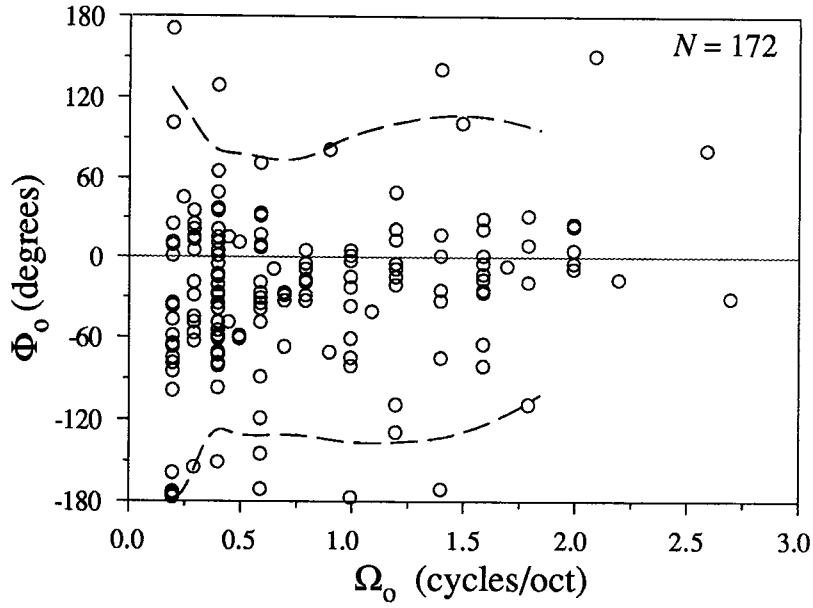
N = 172
180
120
60
0
-60
-120
-180
0.0
0.5
1.0
1.5
2.0
2.5
3.0
Φo (degrees)
Ωo (cycles/oct)

Figure 11